Time scale analysis of the homogeneous flame inhibition by alkali metals

Omar Dounia, Olivier Vermorel, Thomas Jaravel, Thierry Poinsot

Time scale analysis of the homogeneous flame inhibition by alkali metals.

O. Dounia[a,*], O. Vermorel[a], T. Jaravel[a], T. Poinsot[b]

[a] *Centre Européen de Recherche et de Formation Avancée en Calcul Scientifique (C.E.R.F.A.C.S)*
[b] *Institut de Mécanique des Fluides de Toulouse (I.M.F.T)*

Abstract

A time scale analysis of the homogeneous flame inhibition problem is carried out to identify the main parameters controlling the gas phase chemical interaction of the alkali metal inhibitors with the flame chemistry. First, kinetic sub-models for the interaction of alkali metals with the flame are analyzed to show that a simplified 2-step inhibition cycle can capture the essential features of this interaction. Second, it is shown that this cycle is auto-catalytic, which explains the high efficiency of alkali metals in inhibiting flames even at low concentrations. Third, the time scales associated to this inhibition cycle are linked to the free flame termination time scale via a non-dimensional parameter characterizing the efficiency of an inhibitor at promoting radical scavenging. It is shown that this parameter accounts for the main trends observed in the literature and can also be used to provide estimates for the chemical flame suppression limit.

Keywords: homogeneous flame inhibition, alkali metals, laminar flames.

Colloquium:

*Corresponding author

Length of the paper determined using Method 1: 5712 words
Length of the paper determined using Method 2: less than 8 pages
Total length of the abstract: 148 words.

1. Introduction

Until the 1970s, industrial safety processes relied heavily on chlorofluorocarbon gases as fire suppressants in ground, sea and air systems [1]. Since then, the threat to Earth's ozone layer of such gases has been established and their production prohibited. Following this ban, intensive research has been conducted to find efficient halon replacements. Alkali metal compounds, such as $(\mathcal{I}\mathrm{HCO_3})_s$ and $(\mathcal{I}_2\mathrm{CO_3})_s$ with $\mathcal{I} = \{K, Na\}$, have received considerable attention because of their higher effectiveness per mass basis compared to the halon 1301 ($\mathrm{CF_3Br}$) [2]. The flame inhibition (flame speed reduction) and flame suppression abilities of these products has been shown experimentally in premixed flame [3–6] and counter-flow flame [7–10] configurations. This led to their wide commercial use as chemical fire suppressants.

When injected as powders, these inhibitors may be viewed as a discrete set of alkali metal particles which undergo thermal decomposition as soon as they penetrate the flame front [11]. This triggers a series of reactions that can involve multiple phase changes. The main decomposition product is the gaseous agent $\mathcal{I}_g$ to which is attributed the chemical effect of the inhibitor. $\mathcal{I}_g$ is the alkali hydroxide $\mathcal{I}OH$ when $\mathcal{I} = \{K, Na\}$ for example. $\mathcal{I}_g$ reacts with the radical species via chain-termination reactions of the form:

$\mathcal{I}_g + R \longrightarrow P$, where R and P denote radical species and stable products respectively. By promoting radical scavenging, $\mathcal{I}_g$ acts as a catalyser of the chain-termination stage. The main source of flame speed reduction in the case of alkali metals is attributed to this catalytic effect, at least for small concentrations of inhibitor [10, 12, 13].

Extensive research has been dedicated to understanding the flame inhibition process. Most studies have so far focused on the gas-phase interaction between the inhibitor and the flame chemistry. They are based on the assumption that the inhibitor completely decomposes early inside the flame front into a gaseous agent.The latter can then be included in the fresh gases composition, thereby leading to a drastic simplification of the flame inhibition problem. This led to the formulation of multiple kinetic models for the interaction of alkali metal containing species with hydrocarbon flame chemistries [6, 10, 12–15]. The inhibition efficiency of these gaseous agents strongly depends on the flame itself (fuel, equivalence ratio, etc...). A clear understanding of the origin of these differences still lacks today since most of these papers focus on either a single flame or a single gaseous agent.

The objective of this paper is to propose a time scale analysis of the homogeneous inhibition problem, based on one-dimensional flame computations, to identify the origin of said differences. First, Section 2 details the set of hypotheses under which gas-phase inhibition arguments are valid. Section 3 presents the chemical mechanisms used to model the gas-phase flame inhibition process. These mechanisms are then simplified in Section 4 to highlight

the existence of an auto-catalytic 2-step cycle that captures the essential features of the flame inhibition process. The auto-catalytic nature of this cycle and its effect on the radical species chemistry are analyzed in Sections 5 and 6 respectively. A critical parameter, linking flame and inhibition time scales, is also identified in these sections and used, in Section 7, to analyze the chemical flame suppression phenomenon.

2. Clarifying the homogeneous inhibition limit

Research on flame inhibition [6, 10, 12–15] has mostly relied on the interaction of the gaseous agent with the flame chemistry (homogeneous inhibition) to explain the experimental results, without clearly stating the set of assumptions under which this approach is valid. An attempt to clarify this issue is provided in this section.

Let $\tau_f = \delta_L/s_L$ be the flame time scale, where δ_L and s_L are the flame thickness and speed respectively. Let $\mathcal{I}_s$ be the solid inhibiting particle. Let τ_m and τ_h be the particle hydrodynamic and thermal relaxation time scales respectively. Let τ_s be the time scale of the surface reaction $\mathcal{I}_s + R' \Longrightarrow \nu_s^g \mathcal{I}_g + P'$, which provides the flame with the gaseous agent $\mathcal{I}_g$. Unfortunately, major uncertainties surround the rate of the reactions involved in the thermal decomposition stage, preventing us from estimating τ_s. The inhibition problem reduces to its homogeneous limit provided that: 1) the flame is not thermally perturbed by the decomposition stage (*i.e.* negligible thermal-radiation and thermal-cooling); 2) the particle thermal and hydrodynamic inertia are negligible (*i.e.* $\tau_m/\tau_f \ll 1$ and $\tau_h/\tau_f \ll 1$); 3) the decomposition reactions are fast (*i.e.* $\tau_s/\tau_f \ll 1$). These requirements are typically fulfilled for dilute

and finely crushed inhibiting powders. Note that violating (2) or (3) may shift the liberation of the gaseous agent towards the burnt gases where the inhibition effect vanishes.

3. Detailed chemical inhibition sub-models

Under the set of hypotheses detailed in Section 2, the impact of the inhibitor reduces to the catalytic effect of the gaseous agent $\mathcal{I}_g$ on the chain termination stage. To analyze this mechanism, potassium and sodium containing inhibitors are considered (for their high effectiveness). In the following, $\mathcal{I}_g = \mathcal{I}OH$ with $\mathcal{I} = \{K, Na\}$. The Kinetic models in [13] and [12] are used to model the catalytic properties of potassium and sodium containing inhibitors respectively. They are composed of a set of reactions for methane/air flame chemistry (GRI-3.0 mechanism [16]) combined with a set of reactions for alkali metal species. The inhibition sub-models include 48 and 38 reactions, and are denoted $48R$ and $38R$, for $\mathcal{I} = K$ and $\mathcal{I} = Na$ respectively. $48R$ and $38R$ were validated against the experimental data of Rosser *et al.* [3] who used finely crushed powders (2 μm) on CH_4/air flames. The inhibition effect of alkali hydroxydes are analyzed using one-dimensional premixed flames, computed with the Cantera [17] software. A flame with given equivalence ratio ϕ is enriched with various values of $Y_{\mathcal{I}OH,u}$ at $T_u = 300\ K$ and $P = 1\ atm$, where the subscript u refers to the unburnt gas side. Of interest is the evolution of the flame consumption speed s_L with $Y_{\mathcal{I}OH,u}$. In this paper, the free flame limit, denoted by the superscript ^{0}, refers to the case $Y_{\mathcal{I}OH,u} = 0$ where no inhibitor is introduced. Figure 1 displays the evolution of the flame speed s_L with $Y_{\mathcal{I}OH,u}$ for $\mathcal{I} = \{K, Na\}$. With $48R$ and

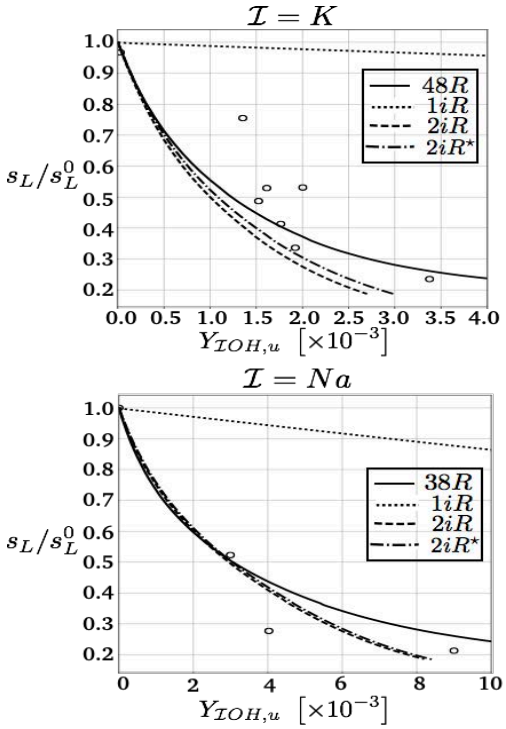

Figure 1: Evolution of the reduced flame speed s_L/s_L^0 with the gaseous agent mass fraction $Y_{\mathcal{I}OH,u}$ for a stoichiometric methane/air flame. s_L^0 is the flame speed at the free flame limit (*i.e.* for $Y_{\mathcal{I}OH,u} = 0$). The circles denote the Rosser *et al.* [3] experimental data.

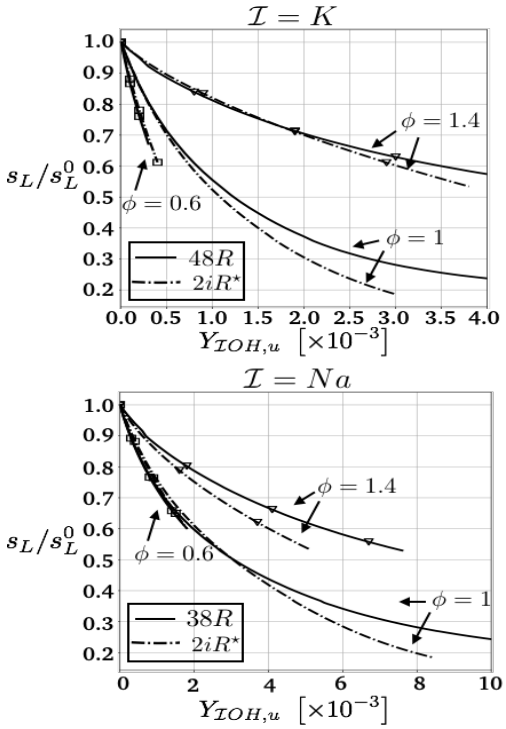

Figure 2: Evolution of the reduced flame speed s_L/s_L^0 with the gaseous agent mass fraction $Y_{\mathcal{I}OH,u}$ for lean ($\phi = 0.6$), stoichiometric and rich ($\phi = 1.4$) methane/air flames.

$38R$ sub-mechanisms, a drastic decrease of the flame speed is observed, which illustrates the catalytic potential of alkali hydroxides. Figure 1 also shows that potassium hydroxyde is more effective, per mass basis, at reducing the flame speed than sodium hydroxide. The results are in fair agreement with the experimental data of Rosser *et al.* [3].

4. The existence of a two-step auto-catalytic inhibition cycle

This section is devoted to the analysis of the inhibition sub-mechanism. One of the most dominant inhibition reactions is the chain termination re-

action:

$$(\mathcal{R}_{\mathcal{I},1}) \quad \mathcal{I}OH + H \Longrightarrow \mathcal{I} + H_2O, \quad k_{\mathcal{I},1} = A_1 f_1(T)$$

where according to [12, 13]:

$$\mathcal{I} = K: \ f_1 = \sqrt{T}, \quad \mathcal{I} = Na: \ f_1 = e^{-991.44/T}$$

By appending $(\mathcal{R}_{\mathcal{I},1})$ to the set of chain-termination reactions, the alkali hydroxide may be viewed as a catalyser of the chain-termination stage. The reaction $(\mathcal{R}_{\mathcal{I},1})$ alone, however, can not explain the drastic flame speed depletion observed with alkali hydroxydes. This is illustrated in Fig. 1, where the detailed inhibition sub-mechanisms are reduced to the sub-models $1iR$ containing only the single irreversible reaction $(\mathcal{R}_{\mathcal{I},1})$. The very mild flame speed depletion observed with $1iR$ is due to the small concentrations $Y_{\mathcal{I}OH,u}$ of alkali hydroxides considered, as will be explained in Section 6. Assuming $\mathcal{I}OH$ to be the primary inhibition agent, there must exist an additional mechanism that can account for the inhibition effect of alkali hydroxide. This additional mechanism is provided by the reaction:

$$(\mathcal{R}_{\mathcal{I},2}) \quad \mathcal{I} + OH + M \Longrightarrow \mathcal{I}OH + M, \quad k_{\mathcal{I},2} = A_2 f_2(T)$$

where, according to [12, 13], $f_2 = 1/T$. Figure 1 shows that the sub-mechanisms $2iR$, composed of only reactions $(\mathcal{R}_{\mathcal{I},1})$ and $(\mathcal{R}_{\mathcal{I},2})$, can fairly reproduce the flame speed reduction observed with the detailed sub-mechanisms $48R$ and $38R$. The reaction $(\mathcal{R}_{\mathcal{I},2})$ allows to regenerate the alkali hydroxide along its path inside the flame front. In this sense, one may say that $(\mathcal{R}_{\mathcal{I},2})$ makes the 2-step inhibition cycle $(\mathcal{R}_{\mathcal{I},1} - \mathcal{R}_{\mathcal{I},2})$ auto-catalytic.

Radical species typically exhibit concentration profiles with a peak around

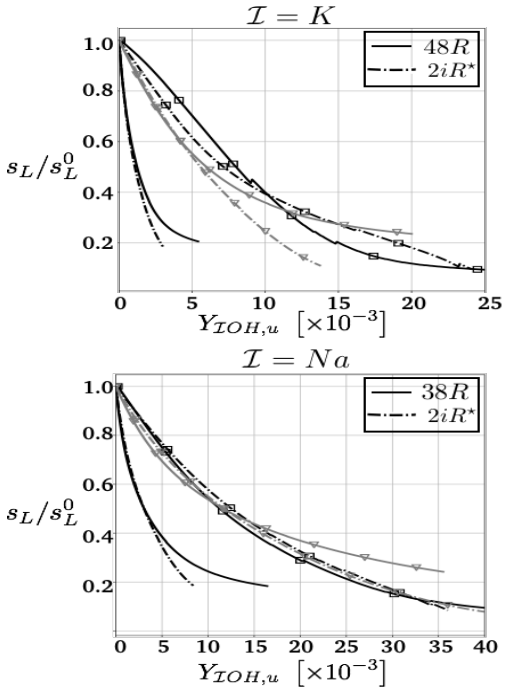

Figure 3: Evolution of the reduced flame speed s_L/s_L^0 with the gaseous agent mass fraction $Y_{\mathcal{I}OH,u}$ for stoichiometric methane/air (no symbol), acetylene/air (triangle symbol) and hydrogen/air (square symbol) flames.

the chain-branching layer of the flame and rapidly relax to zero and their adiabatic equilibrium value on the fresh and burnt gas sides respectively. Therefore, the source terms associated to $(\mathcal{R}_{\mathcal{I},1})$ and $(\mathcal{R}_{\mathcal{I},2})$ are mostly confined around the radical species peak position $x^\star$. This remark combined with the low thermal sensitivity of $k_{\mathcal{I},1}$ and $k_{\mathcal{I},2}$, allows to get rid of the temperature dependance in $k_{\mathcal{I},1}$ and $k_{\mathcal{I},2}$. This thermal insensitivity assumption is useful to define relevant time scales for $(\mathcal{R}_{\mathcal{I},1})$ and $(\mathcal{R}_{\mathcal{I},2})$, as will be done in Section 5. f_1 and f_2 are therefore taken at $T^\star = T^0(x^\star)$, which is defined here as the temperature of a free flame (*i.e.* for $Y_{\mathcal{I}OH,u} = 0$) at the peak H concentration. Let $2iR^\star$ be $2iR$ under this thermal insensitivity approximation:

$$(\mathcal{R}^\star_{\mathcal{I},1}) \quad \mathcal{I}OH + H \Longrightarrow \mathcal{I} + H_2O, \quad k_{\mathcal{I},1} = A_1 f_1(T^\star)$$

$$(\mathcal{R}^\star_{\mathcal{I},2}) \quad \mathcal{I} + OH + M \Longrightarrow \mathcal{I}OH + M, \quad k_{\mathcal{I},2} = A_2 f_2(T^\star)$$

with $M \approx N_2 + 6H_2O$ according to [12, 13]. Figure 1 shows that $2iR^\star$ and $2iR$ predict very similar inhibition effects. Figure 2 shows a reasonable agreement between the detailed inhibition sub-mechanisms and $2iR^\star$ for lean ($\phi = 0.6$) and rich ($\phi = 1.4$) methane/air flames as well.

In an effort to extend the analysis to other fuels, the inhibition sub-mechanisms are now appended to hydrogen/air and acetylene/air mechanisms. In doing so, we implicitly assume the fuel independence of the parameters in $k_{\mathcal{I},1}$ and $k_{\mathcal{I},2}$. The Wang *et al.* [18] and UCSD [19] mechanisms are used here for acetylene and hydrogen flame chemistries respectively. The results are displayed for stoichiometric methane/air, acetylene/air and hydrogen/air flames in Fig. 3. The reduced sub-model $2iR^\star$ captures the essential

features of the flame inhibition process for all selected fuels, thereby validating the thermal insensitivity assumption applied on ($\mathcal{R}_{\mathcal{I},1}$) and ($\mathcal{R}_{\mathcal{I},2}$). Note that for all selected fuels and equivalence ratios, KOH is more effective per mass basis that $NaOH$.

In the following, a time-scale analysis of the homogeneous flame inhibition process is carried out using $2iR^\star$. The auto-catalytic nature of the inhibition cycle is investigated in Section 5, whereas its effect on the radical species chemistry is tackled in Section 6.

5. Estimates for the effective alkali hydroxide concentration

Section 4 highlighted the importance of the alkali hydroxide regeneration mechanism, provided by reaction ($\mathcal{R}^\star_{\mathcal{I},2}$), in the inhibition cycle ($\mathcal{R}^\star_{\mathcal{I},1} - \mathcal{R}^\star_{\mathcal{I},2}$). Obviously, this is possible only for a certain range of $\tau_{\mathcal{I},2}/\tau_{\mathcal{I},1}$, where $\tau_{\mathcal{I},n}$ is the time scale associated to reaction ($\mathcal{R}^\star_{\mathcal{I},n}$). The limiting case is $\tau_{\mathcal{I},2}/\tau_{\mathcal{I},1} \to +\infty$, under which the role of reaction ($\mathcal{R}^\star_{\mathcal{I},2}$) is lost and only a mild inhibition effect may be observed (see the results for $1iR$ in Fig. 1). The regeneration property of reaction ($\mathcal{R}^\star_{\mathcal{I},2}$) can be characterized by the alkali hydroxide mass fraction at the radical pool position $Y^\star_{\mathcal{I}OH} = Y_{\mathcal{I}OH}(T^\star)$. The objective of the present section is to link this effective mass fraction $Y^\star_{\mathcal{I}OH}$ to the mass fraction of $\mathcal{I}OH$ at the fresh gases $Y_{\mathcal{I}OH,u}$ and the parameter $\tau_{\mathcal{I},2}/\tau_{\mathcal{I},1}$.

The validity of the thermal insensitivity assumption on a wide range of

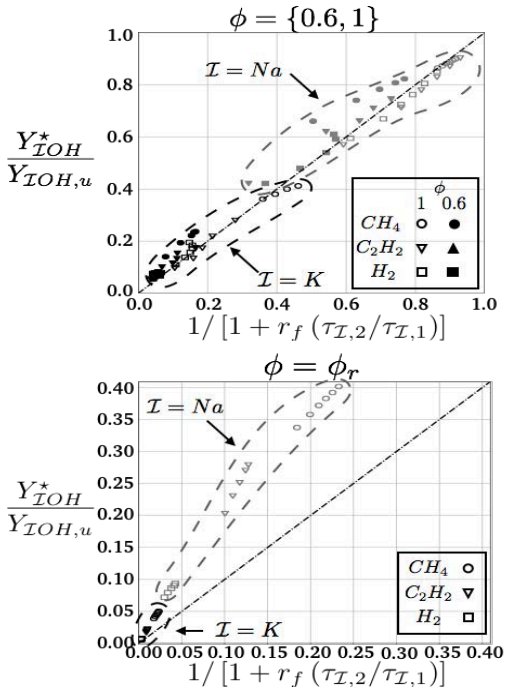

Figure 4: Evolution of the reduced effective alkali hydroxide mass fraction $Y^{\star}_{\mathcal{I}OH}/Y_{\mathcal{I}OH,u}$ with the right hand side of Eq. (4). Gray and black symbols denote $\mathcal{I} = Na$ and $\mathcal{I} = K$ respectively. $\phi_r = \{1.4, 2, 2.5\}$ for CH_4, C_2H_2 and H_2 respectively.

flames allows to introduce two relevant inhibition time-scales:

$$\tau_{\mathcal{I},1} = \frac{W_H}{A_1(\rho f_1)|_{T=T^\star}}, \quad \tau_{\mathcal{I},2} = \frac{W_{N_2} W_{OH}}{A_2(\rho^2 f_2)|_{T=T^\star}} \tag{1}$$

where W_k is the molar mass of species k. Suppose that $\mathcal{I}OH$ and $\mathcal{I}$ species diffusion is negligible compared to convection. The gaseous agent balance equation reads in the flame-attached coordinate system:

$$s_L \frac{dY_{\mathcal{I}OH}}{dx} = \frac{\rho}{\rho_u}\left(-\frac{Y_H Y_{\mathcal{I}OH}}{\tau_{\mathcal{I},1}} + \frac{Y_{OH} Y_{\mathcal{I}} Y_M}{(W_{\mathcal{I}}/W_{\mathcal{I}OH})\tau_{\mathcal{I},2}}\right) \tag{2}$$

$$\text{with,} \quad (W_{\mathcal{I}OH}/W_{\mathcal{I}})Y_{\mathcal{I}} = (Y_{\mathcal{I}OH,u} - Y_{\mathcal{I}OH}) \tag{3}$$

We search for the mass fraction of gaseous agent $Y^\star_{\mathcal{I}OH}$ for which an equilibrium between reaction $(\mathcal{R}^\star_{\mathcal{I},1})$ and $(\mathcal{R}^\star_{\mathcal{I},2})$ is reached around the peak H concentration. Applying a QSS assumption on $\mathcal{I}OH$ $(dY_{\mathcal{I}OH}/dx \approx 0)$ yields the equilibrium inhibition relation:

$$\frac{Y^\star_{\mathcal{I}OH}}{Y_{\mathcal{I}OH,u}} \approx \frac{1}{1 + r_f\,(\tau_{\mathcal{I},2}/\tau_{\mathcal{I},1})}\,, \quad r_f \equiv \frac{Y^\star_H}{Y^\star_{OH} Y^\star_M} \tag{4}$$

r_f is a flame parameter characterizing the relative importance of H and OH radicals inside the chain-branching layer. $\tau_{\mathcal{I},2}/\tau_{\mathcal{I},1}$ is an auto-catalytic term describing the capacity of a given inhibition cycle to maintain non-zero mass of gaseous agent near the radical pool. The reduced effective alkali hydroxide mass fraction $Y^\star_{\mathcal{I}OH}/Y_{\mathcal{I}OH,u}$ is a decreasing function of $\tau_{\mathcal{I},2}/\tau_{\mathcal{I},1}$. As $\tau_{\mathcal{I},2}/\tau_{\mathcal{I},1} \to 0$, $Y^\star_{\mathcal{I}OH} \to Y_{\mathcal{I}OH,u}$ since, in this case, the reaction $(\mathcal{I}^\star_2)$ provides instantaneously one mole of gaseous agent for each mole consumed by the first reaction. On the other hand, as $\tau_{\mathcal{I},2}/\tau_{\mathcal{I},1} \to +\infty$, $2iR$ reduces to $1iR$ thereby breaking the inhibition cycle. In this case $(\mathcal{R}^\star_{\mathcal{I},1})$ proceeds with zero concentration of gaseous agent around $T^\star$.

Figure 4 displays the evolution of the reduced effective alkali hydroxide mass fraction $Y^{\star}_{\mathcal{I}OH}/Y_{\mathcal{I}OH,u}$ with the right hand side of Eq. (4) for hydrogen/air, methane/air and acetylene/air flames. Despite a clear deviation for rich flames, Eq. (4) provides a fair estimate for $Y^{\star}_{\mathcal{I}OH}/Y_{\mathcal{I}OH,u}$. More importantly, it shows that the sodium inhibition cycle is more efficient at regenerating the alkali hydroxide during the inhibition process. Therefore, the higher inhibition efficiency, per mass basis, of the potassium hydroxide (see Fig. 1-3) can not be explained by the regeneration properties of its inhibition cycle. The origin of its higher efficiency is unveiled in Section 6.

6. Time scale analysis of the catalytic properties of alkali metals

Section 5 analyzed the auto-catalytic properties of the inhibition cycle for $\mathcal{I} = \{K, Na\}$ through the effective gaseous agent mass fraction variable $Y^{\star}_{\mathcal{I}OH}$. This section is devoted to the analysis of the impact of $Y^{\star}_{\mathcal{I}OH}$ on the chain termination stage.

Let $\mathcal{R}_T$ be the set of all termination reactions involving the radical H. The chemical source term $\dot{\mathcal{S}}_H$ for the H radical reads around the radical pool:

$$\dot{\mathcal{S}}_H(T^{\star}) = \sum_{r \notin \mathcal{R}_T} \dot{\omega}^{\star}_r + \sum_{r \in \mathcal{R}_T} \dot{\omega}^{\star}_r - \frac{\rho^{\star} Y^{\star}_H Y^{\star}_{\mathcal{I}OH}}{W_{IOH} \tau_{\mathcal{I},1}} \tag{5}$$

Let $\tau_T \equiv 1/(\sum_{r \in \mathcal{R}_T} |\dot{\omega}^{\star}_r|/[H]^{\star})$ be the chain termination time scale, where $[H]$ is the molar concentration of species H. Introducing τ_T to Eq. (5), one

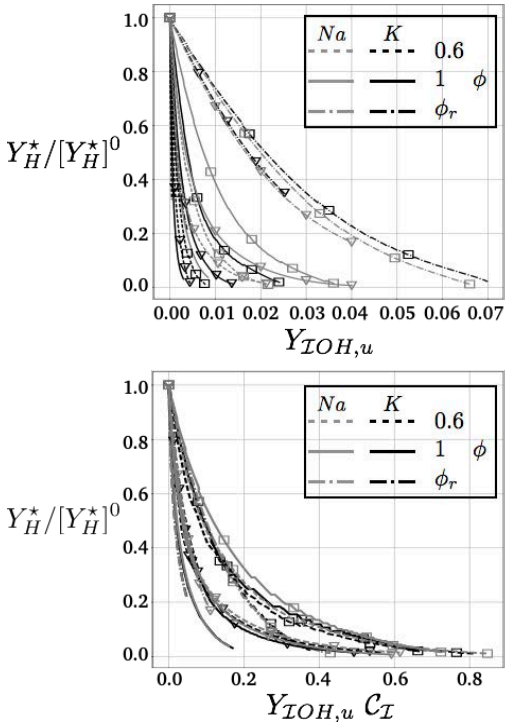

Figure 5: Evolution of the reduced radical peak mass fraction with the mass fraction of gaseous agent $Y_{\mathcal{I}OH,u}$ at the fresh gas side (top) and with the catalytic term in Eq. (6) $Y_{\mathcal{I}OH,u}\ \mathcal{C}_\mathcal{I}$ (bottom) for methane/air (no symbol), acetylene/air (triangle symbol) and hydrogen/air (square symbol) flames.

gets:

$$\dot{\mathcal{S}}_H(T^\star) = \sum_{r \notin \mathcal{R}_T} \dot{\omega}_r^\star - ([H]^\star/\tau_T)\,[1 + Y_{\mathcal{I}OH,u}\,\mathcal{C}_\mathcal{I}] \tag{6}$$

$$\text{with,} \quad \mathcal{C}_\mathcal{I} \equiv (W_H/W_{IOH})(Y^\star_{\mathcal{I}OH}/Y_{\mathcal{I}OH,u})\,(\tau_T/\tau_{\mathcal{I},1}) \tag{7}$$

$\mathcal{C}_\mathcal{I}$ characterizes the efficiency of $\mathcal{I}OH$ at promoting radical scavenging. $\mathcal{C}_\mathcal{I}$ links the free flame termination time scale τ_T to the effective termination time scale τ'_T:

$$\tau_T/\tau'_T \equiv 1 + Y_{\mathcal{I}OH,u}\,\mathcal{C}_\mathcal{I} \tag{8}$$

$\mathcal{C}_\mathcal{I}$ may be written in terms of inhibition parameters using the equilibrium relation (4):

$$\mathcal{C}_\mathcal{I} \approx \frac{(W_H/W_{IOH})\,(\tau_T/\tau_{\mathcal{I},1})}{1 + r_f\,(\tau_{\mathcal{I},2}/\tau_{\mathcal{I},1})} \tag{9}$$

The impact of the inhibition parameters on the chain-termination stage depends on the ratio $\tau_T/\tau_{\mathcal{I},1}$. In the slow inhibition regime, namely $\tau_T/\tau_{\mathcal{I},1} \to 0$, the chain-termination stage is not affected by the presence of the gaseous agent and the inhibition effect vanishes. On the other hand, in the instantaneous inhibition regime ($\tau_T/\tau_{\mathcal{I},1} \to +\infty$, $\tau_{\mathcal{I},2} \neq 0$), $\mathcal{C}_\mathcal{I} \to (\tau_T/\tau_{\mathcal{I},2})/r_f$ and vanishes when no auto-catalytic support is provided by ($\mathcal{R}^\star_{\mathcal{I},2}$) (*i.e.* when $\tau_{\mathcal{I},2}/\tau_T \to +\infty$). This explains the mild flame speed reduction observed in Fig. 1 using the scheme ($1iR$).

Figure 5 shows that when $Y_{\mathcal{I}OH,u}$ is scaled by $\mathcal{C}_\mathcal{I}$, the scavenging effect of the alkali hydroxyde on the H radical exhibits three distinct behaviors, which correspond to the three fuels considered. This shows that, within each fuel,

$\mathcal{C}_{\mathcal{I}}$ accounts for a change in equivalence ratio (via τ_T and r_f) and a change in alkali-metal (via $\tau_{\mathcal{I},1}$, $\tau_{\mathcal{I},2}$ and $W_{\mathcal{I}}$). Note that the differences observed between fuels may be explained by the relative importance of the H radical within each chain-branching kinetics.

Figure 5 shows that the reduced catalytic term $\mathcal{C}_{\mathcal{I}}$ is a well suited variable to analyze the inhibition efficiency of alkali hydroxides. $\mathcal{C}_{\mathcal{I}}$ is displayed in Fig. 6 for the whole set of flames considered in this paper and confronted to relation (9). Using Eq. (9), which provides a fair estimate for $\mathcal{C}_{\mathcal{I}}$, one can explain the main trends observed in the literature. 1) for fixed fuel and ϕ, Fig. 6 shows that $\mathcal{C}_K > \mathcal{C}_{Na}$, despite weaker auto-catalytic support ($\tau_{K,2}/\tau_{K,1} > \tau_{Na,2}/\tau_{Na,1}$, see Fig. 4). Therefore, the origin of the higher inhibition efficiency of potassium hydroxide lies in faster H scavenging reaction ($\mathcal{R}_{\mathcal{I},1}$) (*i.e.* higher $\tau_T/\tau_{\mathcal{I},1}$). 2) For fixed fuel and $\mathcal{I}$, Fig. 6 shows that $\mathcal{C}_{\mathcal{I}}$ is a decreasing function of ϕ, which may be explained mostly by stronger relative radical pool r_f as ϕ increases. For fixed inhibitor parameters, r_f dictates the balance between $\mathcal{I}OH$ consumption and regeneration rates (see Eq. (2)), thereby controlling the effective $\mathcal{I}OH$ mass fraction, which as stated in Eq. (4) is a decreasing function of r_f. 3) Finally, Fig. 6 shows that, for fixed $\mathcal{I}$ and ϕ, $\mathcal{C}_{\mathcal{I}}$ is higher for CH_4 in comparison with more reactive fuels like H_2, which is attributed here to lower r_f.

7. Chemical flame suppression phenomenon

As shown in Section 6, the catalytic effect of a given chemical inhibitor on the chain termination stage may be described using $\mathcal{C}_{\mathcal{I}}$ which, according to

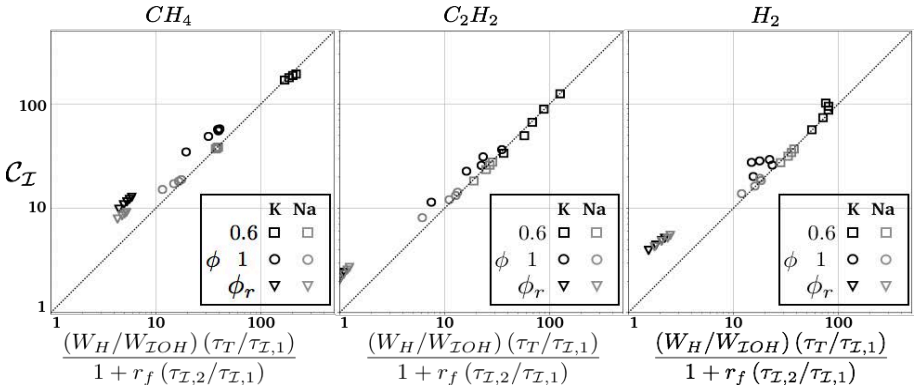

Figure 6: Evolution of the reduced catalytic term $\mathcal{C}_\mathcal{I}$, defined in Eq. (7), with the right hand side of Eq. (9). $\phi_r = \{1.4, 2, 2.5\}$ for CH_4, C_2H_2 and H_2 respectively.

Eq. (8), increases the overall rate of the chain termination reactions τ_T/τ'_T . τ_T/τ'_T admits an upper bound above which no flame can be sustained. This upper bound corresponds to the chemical suppression limit. It is reached when the source term in Eq. (6) vanishes, *i.e.* when the radical termination rate equates its creation rate. Let $\mathcal{R}_c = \mathcal{R}\backslash\mathcal{R}_T$ be the set of reactions responsible for the production of H, which includes mostly chain initiation and chain-branching reactions. Let τ_c be the creation time scale, defined by $\tau_c \equiv 1/(\sum_{r\in\mathcal{R}_c} |\dot{\omega}^\star_r|/[H]^\star)$. τ_c is computed at the free flame limit. Chemical flame suppression is thus achieved for $\tau_T/\tau'_T = \tau_T/\tau_c$. Using Eq. (9), this provides an estimate for the minimum mass of gaseous agent $Y^s_{\mathcal{I}OH,u}$ able to chemically suppress a given flame:

$$Y^s_{\mathcal{I}OH,u} \approx (\tau_T/\tau_c - 1)/\mathcal{C}^0_\mathcal{I} \tag{10}$$

where $\mathcal{C}_\mathcal{I}$ is taken at the free flame limit for simplicity. According to Eq. (10), $Y^s_{\mathcal{I}OH,u}$ is a decreasing function of $\mathcal{C}^0_\mathcal{I}$, which simply means that a set of flame and inhibitor characterized by high catalytic potentiel (high $\mathcal{C}^0_\mathcal{I}$) would

require few mass of gaseous agent to reach flame suppression. Equation (10) predicts that $Y^s_{KOH,u} = 0.0017$ ($Y^s_{KOH,u} = 0.013$) is needed to suppress a stoichiometric CH_4/air (H_2/air *resp.*) flame, in fair agreement with the values extracted from the 1D-simulations: 0.003 and 0.024 respectively. The fact that $Y^s_{KOH,u}$ is lower for CH_4 in comparison with H_2 is attributed here to lower termination to creation time scale ratio τ_T/τ_c and higher catalytic potential (*i.e.* higher $\mathcal{C}^0_{\mathcal{I}}$).

8. Conclusion

A time scale analysis of the homogeneous flame inhibition problem has been conducted in this paper to identify the main parameters controlling the gas phase chemical interaction of the inhibitor with the flame chemistry. First, proposed sub-models for the interaction of alkali metals with the flame have been analyzed to highlight the existence of a 2-step inhibition cycle that captures the essential features of this interaction. It is shown that the cycle is auto-catalytic which explains the high efficiency of alkali metals in inhibiting flames even at low concentrations.

The autocatalytic efficiency of this 2-step cycle is characterized by the effective alkali hydroxide mass fraction $Y^\star_{\mathcal{I}OH}$ around which the inhibition reactions take place. A time scale analysis of the H radical conservation equation, based on this effective agent mass fraction $Y^\star_{\mathcal{I}OH}$, allows to explain the catalytic effect of this 2-step cycle on the chain-termination reactions using a single non-dimensional variable $\mathcal{C}_{\mathcal{I}}$. $\mathcal{C}_{\mathcal{I}}$ is a reduced catalytic term linking the time scales of the inhibition reactions to the time scale of the free-flame chain termination stage. The scavenging effect of the inhibitor on the H

radical becomes quasi self-similar when displayed on the $\mathcal{C}_{\mathcal{I}}$ axis for fixed fuel, which shows that this catalytic term is well suited for the analysis of the homogeneous flame inhibition process rather than $Y_{\mathcal{I}OH,u}$ usually used in the flame inhibition community.

Finally, $\mathcal{C}_{\mathcal{I}}$ is used to provide estimates for the minimum mass of inhibitor $Y^s_{\mathcal{I}OH,u}$ able to chemically suppress a given flame. Chemical flame suppression may be achieved when the radical H is consumed to the point where no radical pool is observed. $Y^s_{\mathcal{I}OH,u}$ reproduces all the important trends observed numerically.

Note that the extension of the present study to other inhibitors may require further analysis of their associated inhibition sub-mechanisms. More complex approaches than the one proposed in this paper could most assuredly be mandatory in the study of more complex gaseous agents. A partial equilibrium approximation can, for example, be applied to the system of inhibition species and radical reactions, leading to a more accurate description of the inhibition process. Also, it is important to stress that this analysis is based on the strong instantaneous thermal decomposition assumption, which may hardly be valid under most relevant conditions.

Acknowledgments

The authors would like to thank Dr. L. Hoorelbeke and Dr. A. Dutertre for many fruitful discussions on the flame inhibition process and Total company for supporting this work.

References

[1] D. Trees, K. Seshadri, Experimental studies of flame extinction by sodium bicarbonate (NaHCO3) powder, Combust. Sci. Technol. 122 (1997) 215–230.

[2] A. Hamins, Flame extinction by sodium bicarbonate powder in a cup burner, Twenty-Seventh Symposium (International) on Combustion, The Combustion Institute, Pittsbutgh (1998) 2857–2864.

[3] W. Rosser, S. Inami, H. Wise, The effect of metal salts on premixed hydrocarbon—air flames, Combust. Flame 7 (1963) 107–119.

[4] M. Dewitte, J. Vrebosch, A. van Tiggelen, Inhibition and extinction of premixed flames by dust particles, Combust. Flame 8 (1964) 257–266.

[5] P. Laffitte, R. Delbourgo, J. Combourieu, J. Dumont, The influence of particle diameter on the specificity of fine powders in the extinction of flames, Combust. Flame 9 (1965) 357–367.

[6] K. S. Iya, S. Wollowitz, W. E. Kaskan, The mechanism of flame inhibition by sodium salts, Fifteenth Symposium (International) on Combustion, The Combustion Institute, Pittsbutgh (1975) 329–336.

[7] R. Friedman, J. Levy, Inhibition of opposed jet methane-air diffusion flames. the effects of alkali metal vapours and organic halides, Combust. Flame 7 (1963) 195–201.

[8] M. Vanpee, P. Shirodkar, A study of flame inhibition by metal com-

pounds, Seventeenth Symposium (International) on Combustion, The Combustion Institute, Pittsbutgh (1979) 787–795.

[9] M. Vanpee, P. P. Shirodkar, Characterization of physical, thermal and chemical contributions of sodium bicarbonate particles in extinguishing counterflow nonpremixed flames, 5th ASME/JSME Thermal Engineering Joint Conference (1999).

[10] H. Chelliah, P. Wanigarathne, A. Lentati, R. Krauss, G. Fallon, Effect of sodium bicarbonate particle size on the extinction condition of nonpremixed counterflow flames, Combust. Flame 134 (2003) 261–272.

[11] O. Dounia, O. Vermorel, T. Poinsot, Theoretical analysis and simulation of methane/air flame inhibition by sodium bicarbonate particles, Combust. Flame 193 (2018) 313–326.

[12] V. Babushok, K. McNesby, A. Miziolek, R. Skaggs, Modeling of synergistic effects in flame inhibition by 2-H heptafluoropropane blended with sodium bicarbonate, Combust. Flame 133 (2003) 201–205.

[13] V. I. Babushok, G. T. Linteris, P. Hoorelbeke, D. Roosendans, K. van Wingerden, Flame inhibition by potassium-containing compounds, Combust. Sci. Technol. 189 (2017) 2039–2055.

[14] B. A. Williams, J. W. Fleming, Suppression mechanisms of alkali metal compounds, in: Proceedings of the 1999 Halon Options Technical Working Conference, pp. 157–169.

[15] B. A. Williams, J. W. Fleming, CF_3Br and other suppressants: Differences in effects on flame structure, Proc. Combust. Inst. 29 (2002) 345–351.

[16] G. P. Smith, D. M. Golden, M. Frenklach, N. W. Moriarty, B. Eiteneer, M. Goldenberg, C. T. Bowman, R. K. Hanson, S. Song, J. William C. Gardiner, V. V. Lissianski, Z. Qin, GRI-Mech 3.0 http://www.me.berkeley.edu/gri_mech/, 2017.

[17] D. G. Goodwin, R. L. Speth, H. K. Moffat, B. W. Weber, Cantera: An object-oriented software toolkit for chemical kinetics, thermodynamics, and transport processes, https://www.cantera.org, 2018. Version 2.3.0.

[18] H. Wang, A. Laskin, Z. Djurisic, C. Law, S. Davis, D. Zhu, A comprehensive mechanism of C_2Hx and C_3Hx fuel combustion, in: Fall Technical Meeting of the Eastern States Section of the Combustion Institute, Raleigh, pp. 129–132.

[19] P. Saxena, F. A. Williams, Testing a small detailed chemical-kinetic mechanism for the combustion of hydrogen and carbon monoxide, Combust. Flame 145 (2006) 316 – 323.